processes

MDPI

Article

Evaluation of XD 10 Polyamide Electrospun Nanofibers to Improve Mode I Fracture Toughness for Epoxy Adhesive Film Bonded Joints

Stefania Minosi *, Fabrizio Moroni and Alessandro Pirondi

Department of Engineering and Architecture, University of Parma, Parco Area delle Scienze 181/A, 43124 Parma, Italy
* Correspondence: stefania.minosi@unipr.it

Abstract: The demand for ever-lighter structures raises the interest in bonding as a joining method, especially for materials that are difficult to join with traditional welding and bolting techniques. Structural adhesives, however, are susceptible to defects, but can be toughened in several ways: by changing their chemical composition or by adding fillers, even of nanometric size. Nanomaterials have a high surface area and limited structural defects, which can enhance the mechanical properties of adhesives depending on their nature, quantity, size, and interfacial adhesion. This work analyzes the Mode I fracture toughness of joints bonded with METLBOND® 1515-4M epoxy film and Xantu-Layr electrospun XD 10 polyamide nanofibers. Two joint configurations were studied, which differed according to the position of the nanomat within the adhesive layer: one had the nanofibers at the substrate/adhesive interfaces, and the other had the nanofibers in the center of the adhesive layer. Double cantilever beam joints were manufactured to evaluate the Mode I fracture toughness of the bonding with and without nano-reinforcement. The nanofibers applied at the substrate/adhesive interface improved the Mode-I fracture toughness by 32%, reaching the value of 0.55 N/mm. SEM images confirm the positive contribution of the nanofibers, which appear stretched and pulled out from the matrix. No fracture toughness variation was detected in the joints with the nanofibers placed in the middle of the adhesive layer.

Keywords: bonded joints; bonding reinforcement; nanomaterials; fracture toughness; epoxy; electrospinning

Citation: Minosi, S.; Moroni, F.; Pirondi, A. Evaluation of XD 10 Polyamide Electrospun Nanofibers to Improve Mode I Fracture Toughness for Epoxy Adhesive Film Bonded Joints. *Processes* **2023**, *11*, 1395. https://doi.org/10.3390/pr11051395

Academic Editor: Raul D. S. G. Campilho

Received: 30 March 2023
Revised: 20 April 2023
Accepted: 25 April 2023
Published: 4 May 2023

1. Introduction

Advanced composite materials are commonly used for various applications due to their high strength-to-weight ratio. Glass fiber-reinforced polymers (GFRPs), carbon fiber-reinforced polymers (CFRPs), and sandwich structures are widely used in the aerospace, automotive, marine, and railway industries, as well as in the production of wind blades and sports equipment. The development of these materials has led to the advancement of structural adhesives and bonding techniques [1–5] used to join complex and multi-material structures, replacing traditional mechanical fastening [6–8]. Composite materials, metal fiber laminates, sandwich composites, and adhesive joints are subject to delamination. This refers to interlayer failure in the case of composite laminates, while for metal fiber laminates, sandwiches, and bonded joints, it refers to interface failure [9–11]. However, adhesive bonding is prone to delamination failure under high peel loads, which can be improved by developing new adhesive materials and bonding techniques [11].

Epoxy adhesive is widely used as a structural adhesive. However, in its neat formulation, it undergoes brittle fracturing, with a low fracture toughness, which represents a significant limitation for its application in the structural field [11,12]. Joints bonded with brittle epoxy adhesive are defect-sensitive and exhibit broad strength dispersion due to scatter in flaw sizes. To enhance the toughness of structural adhesives, particularly epoxy

systems, various methods are commonly employed, such as adding fillers or thermally expandable particles (TEPs), or modifying the chemical resin composition [13–15].

The addition of rubber is also a common method used to enhance the fracture toughness of adhesives [16]. The rubbery phase can be introduced in the form of cross-linked [17,18] or core–shell rubbery particles [19], or liquid rubber can be mixed with resin precursors to allow the precipitation of rubbery particles during resin cross-linking [18,20]. To achieve the toughening effect for epoxy systems, a rubbery fraction between 5 and 20 wt. % is added. However, adding a high amount of rubber can lead to a reduction in the glass transition temperature (Tg), elastic modulus, and strength of the resin [21].

Adding organic and inorganic fillers, such as metallic micro- and nano-particles, nanoclays or short fibers, is another method used to improve the fracture toughness of structural adhesives [13,22–24]. Nanoparticles can also increase the fracture toughness, strength, and stiffness of bonded joints [13]. However, it is crucial to develop a strong interfacial adhesion to correctly transfer the load from the polymeric matrix to the nano-reinforcement [13]. Carbon-based nanoparticles, such as carbon nanofibers (CNFs), carbon nanotubes (CNTs) and graphene nanoplatelets (GNPs), are widely used for this purpose [25–39]. These nanoparticles enhance the fatigue life of bonded joints and can be used for damage detection, as they also improve the electrical properties of the resin they are dispersed in [29–39]. Recently, studies have shown that the application of hybrid nanoparticles is a viable approach to designing tougher, stronger and more durable bonded joints [40–44].

The integration of polymeric nanofibers has been shown to be an effective method for toughening epoxy matrices and composite materials [45]. Many studies have shown that composite laminates reinforced with electrospun polymeric nanofibers exhibit enhanced mechanical properties, including improved fracture toughness and delamination strength, with the interposition of a thermoplastic nanomat between composite layers promoting the ply-to-ply bridging effect [46–53]. Hamer et al. studied laminates of CFRP interleaved with electrospun Nylon 66 nanofibers. They performed DCB tests to evaluate the effects of the nanofibers on Mode I fracture toughness. The mat of naofibers embedded in the midplane improved the toughness by about 3 times [47]. Beckermann and Pickering studied the effects of interleaved nanofiber plies on the mode I and mode II interlaminar fracture toughness of carbon and epoxy resin laminates. Various types of electrospun nanofibers were placed in the midplane planes of the laminates. The results show that the best performance was achieved using 4.5 g/m^2 PA66 ply, with fracture toughness improvements of 156% and 69% for Mode I and Mode II, respectively [49]. Saghafi et al. studied the effect of Nylon 6,6 nanofibers interleaved in the midplane of glass/epoxy laminates on mode I and mode II fracture toughness. Nylon 6,6 nanofibers improved the initial G_{IC} and G_{IIC} energy release rates by 62% and 109%, respectively [50]. Daelemans et al. demonstrated that nanofibrous veils of PA 6.9 with different morphologies interleaved in UD carbon/epoxy laminates cause an increase in mode II interlaminar fracture toughness. Mode II interlaminar fracture toughness is doubled by randomly deposited PA 6.9 nanofibers [51]. Goodarz et al. demonstrated that the interfacial incorporation of aramid nanofibers significantly increases the absorbed impact energy, compared to laminates without nanofibers [54].

These results suggest that polymeric nanofibers could be effective in improving crack toughening for bonded joints as well. There have been limited studies on the use of electrospun nanofibers in adhesive bonding, particularly with medium–low-fracture toughness epoxy resins [55–58]. The works [55,56] analyze the effect of a core/shell structure of electrospun meta-aramid fibers integrated into the adhesive layer of the epoxy-bonded joint. Single-lap shear test results show that electrospun meta-aramid nanofibers decreased joint strength, while those with core/shell structure restored the strength of pure epoxy. Razavi et al. found that incorporating polyacrylonitrile (PAN) nanofibers into an aluminum DCB joint bonded with 2k epoxy resin resulted in a two-fold increase in fracture toughness [57]. Ekrem and Avci demonstrated that incorporating polyvinyl alcohol (PVA) nanofibrous mats into the adhesive layer of single lap joints (SLJ) and DCB joints improved shear strength by 13.5% and increased mode I fracture toughness by about two times that of the

neat adhesive [58]. In a previous work, the authors demonstrated that electrospun nylon nanofibers can act as reinforcements and support for the adhesive layer, improving the fracture toughness of low-toughness resins in DCB joints made with pre-impregnated nanofibers [59–62]. In a previous work, impregnation of the nanofibers was initially performed with low- and medium-viscosity epoxy resins to facilitate the wetting of the nanomat [59]. Then, an unfilled medium viscosity two-component epoxy adhesive was used before using a high-viscosity, high-strength two-component epoxy adhesive system [60–62]. However, tests performed on bonded joints were characterized by extensive areas of adhesive failure, at the interface between substrate and adhesive. The improvement of interfacial adhesion is critical for the evaluation of the effect of nanofibrous structures.

Despite the non-marginal scientific literature on the application of nanofibers for interface toughening, the application to adhesive bonding is still limited, and in-house procedures for the embedding are used, for which the possibility of scaling up to an industrial level is either impractical or unclear. Additionally, home-made electrospun nanofibers are often used, which may have a more limited reproducibility than when manufactured on an industrial scale.

Based on the previous considerations, this study investigates the effect of commercial XD 10 polyamide electrospun nanofibers (XantuLayr™, NANOLAYR LTD, Auckland, New Zealand) on composite joints bonded with epoxy film, commonly used in the aerospace industry. The XantuLayr nanomat is known to improve the interlaminar fracture toughness of composite laminates, resulting in higher delamination resistance and damage tolerance [49,53].

In this work, a XantuLayr electrospun nanomat was used for the first time as a toughening element of composite adhesive joints made by secondary bonding. Furthermore, the joints were produced using bonding techniques employed in the automotive and aerospace industries, and were thus compatible with current industrial practices. The manufacturing technique of these joints is therefore replicable in an industrial environment and not just on a laboratory scale. In this work, two joint configurations were studied: one with nanofibers applied at the adhesive/adherend interfaces, and one with nanofibers placed in the center of the adhesive layer. Double Cantilever Beam (DCB) joints were produced to evaluate the mode-I fracture toughness of the bond with and without nano-reinforcement. A morphological analysis was also performed to understand the phenomena occurring during crack propagation.

2. Materials and Method

2.1. Adherends

In this study, CYCOM® 977-2 prepreg (Solvay Specialty Polymers SpA, Bollate (MI), Italy) was used to fabricate composite adherents. This prepreg is suitable for aerospace and aircraft applications that require impact resistance and light weight. The unidirectional tape used had a nominal thickness of 0.186 mm and a density of 1.55 g/cm^3. A quasi-isotropic laminate was produced using 32 layers of prepreg with a lamination sequence of $[45/0/–45/90]_{4s}$. The panels were prepared for bonding using a peel ply, a sacrificial layer of fabric put on the surface of the composite. The panel was vacuum-bagged and cured in an autoclave using the cycle specified by the prepreg technical datasheet. The vacuum bag was realized as reported in Figure 1. After curing, the part was debagged and cut to size. The peel ply was removed from the panel surface prior to bonding.

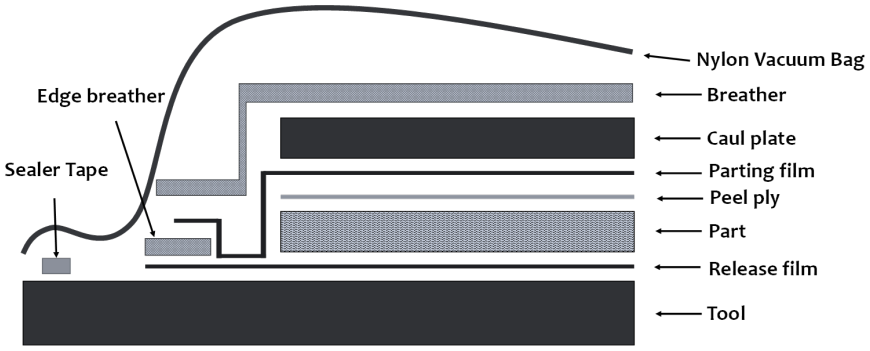

Figure 1. Vacuum bag.

The elastic modulus of the laminate was evaluated to be 58 GPa using tensile testing in accordance with the ASTM D3039 standard [63].

2.2. Adhesive

The epoxy adhesive used for the joint fabrication was the METLBOND® 1515-4M (Solvay Specialty Polymers SpA, Bollate (MI), Italy). This adhesive is mainly employed for bonding composites, although it is suitable for various metal bonding applications. The adhesive has a nominal weight of 242 g/m^2, with a nylon web carrier accounting for 7.5% of the total weight of the film. The elastic modulus of the adhesive film is closely related to the curing pressure and temperature. Based on recommendations from the supplier and various studies in the literature, the elastic modulus of METLBOND® 1515-4M was determined to be 3.5 GPa [64–66]. The yield strength, ultimate strength and strain at failure of the adhesive were not available in the data sheet and, since they are not essential to the purposes of the work and the manufacturing of a tensile test specimen out of a film adhesive is not straightforward, they were not evaluated.

The curing cycle for the bonded joints included an autoclave at 6 bar pressure at 180 °C for 210 min. This cycle is similar to that proposed by the adhesive manufacturer's datasheet, and is the same as that employed for the adherents' manufacturing. The chosen cure cycle is of industrial significance as it enables the consolidation and cure of prepreg and secondary bonding simultaneously, leading to time and energy savings, and it is suitable for co-bonded joints.

2.3. Nanofibers

XantuLayr® (NANOLAYR LTD, Auckland, New Zealand) is a thermoplastic nanofiber veil produced using Sonic Electrospinning Technology. It consists of XD10 polyamide nanofibers that form an ultra-thin non-woven web. For this study, a XantuLayr® nanomat with an areal density of 3 g/m^2 was used. The thickness of the nanomat was measured using a digital indicator (ALPA, Pontoglio (BS), Italy), with a preload of 0.65 N, and was found to be in the range of 120 to 160 μm.

2.4. Double Cantilever Beam Fabrication

To assess the impact of integrating commercial nanofibers on the fracture toughness of the adhesive system, four series of DCB joints were manufactured. Table 1 and Figure 2 provide details of the various configurations of the DCB joints.

Table 1. Composite DCB joints configurations.

Series ID	Adhesive Layer	Number of Samples
1S	METLBOND® 1515-4M	7
2S	2 METLBOND® 1515-4M	8
1S–2NF	XantuLayr® + METLBOND® 1515-4M + XantuLayr®	8
2S–1NF	METLBOND® 1515-4M + XantuLayr® + METLBOND® 1515-4M	8

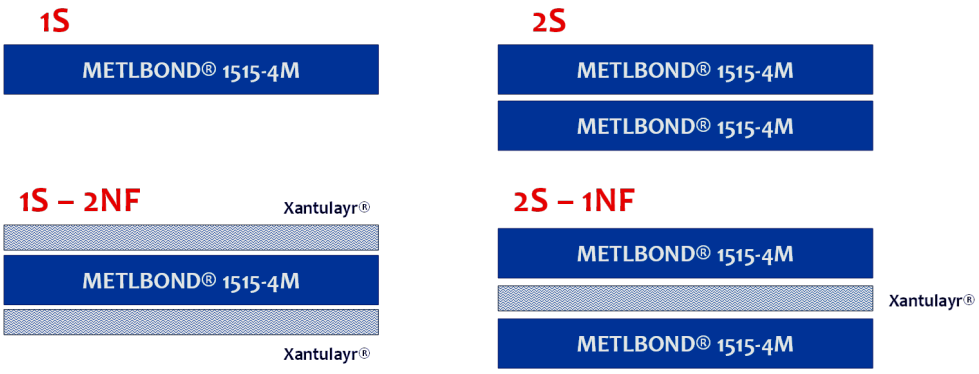

Figure 2. Configurations of the adhesive layers.

The four configurations chosen were 1S, 2S, 1S–2NF and 2S–1NF. The 1S and 2S configurations refer to the virgin specimens, bonded with one and two layers of adhesive, respectively. The 1S–2NF and 2S–1NF configurations refer to the bonded joints reinforced with nanofibers. The 1S–2NF configuration involves the positioning of nanofibers at the adhesive/support interfaces of joints bonded with one layer of adhesive. The 2S–2NF configuration involves the positioning of nanofibers at the center of the adhesive layer of joints bonded with a layer of epoxy film.

The number of samples was defined in such a way as to derive at least five useful samples for calculating the average fracture toughness value and assessing the repeatability of the failure type.

To manufacture the specimens for testing, two composite panels measuring 190 × 150 mm^2 were bonded together and placed in a vacuum bag. A peel-ply was used in the preparation of the panels, which was then removed after the composite had cured, prior to bonding. This method proved to be an effective means of ensuring a strong bond between the composite parts. The joint curing process was carried out in an autoclave at 6 bar pressure and 180 °C temperature for 210 min. During the bonding stage, a 25 mm initial defect was introduced by placing a 0.1 mm-thick Teflon patch on one end of the joint. The nanofibers were placed manually on the adhesive film. Since they were supported on a paper backing, they were easy to handle. Once the nanofibers were properly positioned, the paper backing was removed. After curing, the panels were cut to form DCB joints with a length of 150 mm and width of 25 mm. Two pairs of bonded panels were manufactured for each configuration. Holes were machined for each joint to enable the attachment of steel blocks, which were utilized to secure the specimen in the testing apparatus. Steel blocks were glued to the DCBs using Loctite Hysol 9466 adhesive. To ensure the correct positioning of the blocks, they were fastened to the adherents with screws and bolts. Once the adhesive was polymerized after 24 h at room temperature, screws and nuts were removed, and the DCB was ready to be tested. The adherent dimensions were reduced if compared with ASTM D3433 standards. These dimensions were chosen on the basis of the available material. The DCB geometry is illustrated in Figure 3. Figures 4 and 5 show an example of a tested specimen and the same one mounted on the test machine.

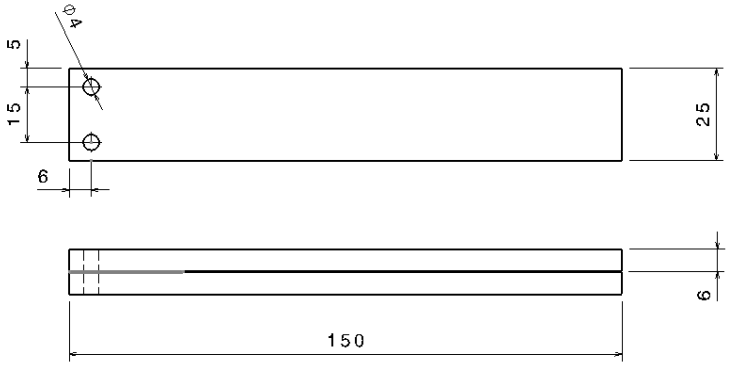

Figure 3. Composite DCB geometry.

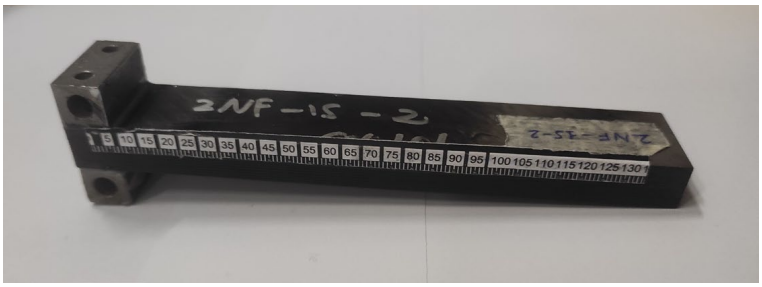

Figure 4. Example of a DCB specimen.

Figure 5. Specimen mounted on the testing machine.

The Table 2 shows the average thicknesses of the tested specimens. The calculation of the adhesive layer's thickness was carried out using the difference between the average joint thickness and the average thickness, t, of the individual adhesives. The presence of the nylon cloth inside the adhesive layer ensures joints with a constant adhesive cross-section.

Table 2. Samples thickness.

Sample ID	t (mm)
1S	0.17
2S	0.48
1S–2NF	0.18
2S–1NF	0.52

2.5. DCB Test

The DCB test was conducted on a servo-hydraulic MTS 810 machine with a 3 kN load cell, using displacement control at a constant crosshead velocity. The loading and unloading rates were 2 mm/min and 5 mm/min, respectively. The correct determination of mode I fracture toughness is crucial to assess the integration effect of the nanomaterial. There are several data reduction methods that can be used to overcome the problem of direct crack length monitoring during the DCB test. The data reduction schemes include the compliance calibration method, in which compliance is calibrated as a polynomial function of crack length, and the compliance-based beam method, which considers the influence of the fracture process zone [67–69]. In this paper, according to the same procedure used in the past by the authors, partial unloadings are performed to determine the specimen compliance and actual crack length using Krenk's model, reported in [70], which accounts for the out-of-plane deformation of the adhesive layer and rotation at the crack tip. The model is represented by Equation (1):

$$C = \frac{\delta'}{P} = 2\left[\frac{2\lambda_\sigma}{k}(1+\lambda_\sigma a) + (a+g)\frac{(2\lambda_\sigma^2)}{k}(1+2\lambda_\sigma a) + \frac{a^3}{3EJ} + g\frac{a^2}{2EJ}\right] \quad (1)$$

The joint compliance (C (mm/N)) is determined by dividing the Crack Mouth Opening Displacement (CMOD) measurement at the front of the specimen (δ' (mm)) by the load (P (N)). Other variables in the equation include the actual crack length (a (mm)), Young's modulus of the adherents (E (MPa)), and area moment of inertia of the adherent (J (mm^4)). A clip gage was used to measure the CMOD during testing. The model presented in Equation (1) has been modified from the one proposed by Krenk to account for the distance (g (mm)) between the measurement point and the load axis, as well as the effect of shear.

The joint geometry is shown in Figure 6.

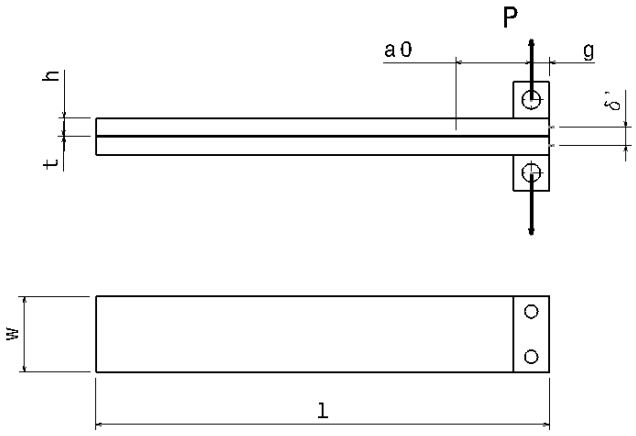

Figure 6. DCB geometry [71,72], where a_0 is 25 mm and g is 6 mm.

The dimensionless parameters λ_σ and k are reported in Equations (2) and (3):

$$\lambda_\sigma = \sqrt[4]{\frac{6}{h^3 t}\frac{E_a}{E(1-v_a^2)}} \quad (2)$$

$$k = \frac{2E_a t}{t\,(1 - v_a^2)} \tag{3}$$

where all the sizes are expressed in mm, while *Ea* (MPa) and v_a (dimensionless) are the Young's modulus and the Poisson's ratio of the adhesive, respectively. The Mode *I* strain energy release rate *G* (N/mm) is:

$$G_I = \frac{(Pa)^2}{tEJ}\left(1 + \frac{1}{\lambda_\sigma a}\right)^2 \tag{4}$$

Since the fiber volume fraction is negligible, for the rule of mixtures, the Young's modulus of the nanomat prepreg is also approximately the same as that of the adhesive alone.

3. Results and Discussion

Figures 7–9 show the load against CMOD of virgin and nanomodified specimens 1S, 2S, 1S–NF and 2S–1NF, taken as representative. The load peaks of virgin samples are slightly lower than 600 N, and the employment of two layers instead of one does not significantly affect adhesive performance. The nanomodified sample has a slightly higher load peak than the neat joint during crack propagation, and the behavior of the 2S–1NF joint is comparable to that of the virgin samples.

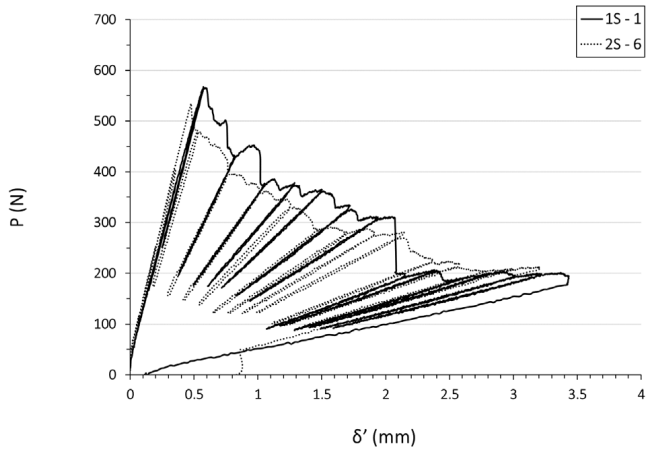

Figure 7. Load against CMOD (δ') for virgin specimens 1S–1 and 2S–6.

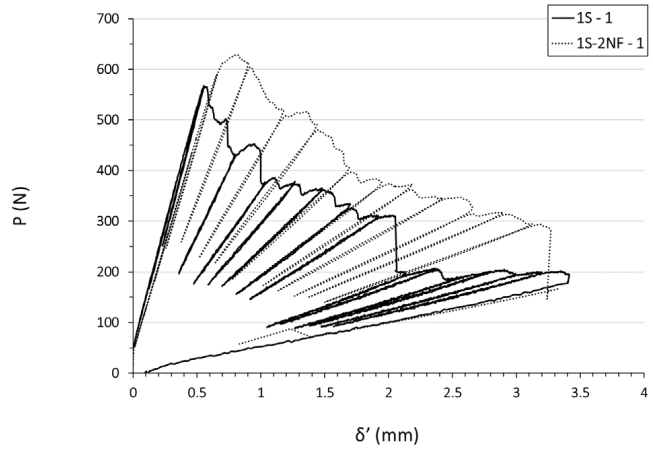

Figure 8. Load against CMOD (δ') for both virgin (1S–1) and nylon-nanomodified (1S–2NF–1) specimens.

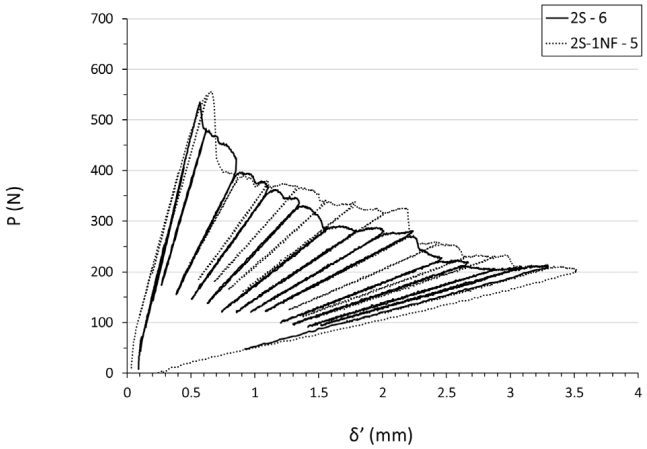

Figure 9. Load against CMOD (δ') for both virgin (2S–6) and nylon-nanomodified (2S–1NF–5) specimens.

Figure 10 displays the fracture surfaces of 1S, 2S, 1S–2NF, and 2S–1NF samples. As can be seen from the picture, the fibers of the bonded surface are at 45°. This solution was preferred as it represents a more general case of joining. The blue areas highlight the presence of the adhesive on the substrate under examination. The 1S specimens failed cohesively during the first stage of the crack propagation, but the crack deviated inside the composite support generally after 30 mm of propagation inside the adhesive. The failure mode of 2S samples was more scattered, with cohesive failure observed in joints 2S–1, 2S–4, and 2S–5 in the initial stage of crack propagation, interfacial fracture in joints 2S-2 and 2S-3, and cohesive fracture in joints 2S–6, 2S–7, and 2S–8. Figure 11 shows SEM images of the fracture surfaces of the 1S–1 and 2S–6 samples, respectively, which show micro-dimples and broken nylon fibers. The 1S–2NF specimens failed cohesively, but the crack deviated inside the composite supports of the samples 1S–2NF 3, 4 and 5 after 30 mm of propagation inside the adhesive. Samples 2S–1NF exhibited cohesive failure, but half of them were subjected to crack propagation inside the composite layer at Δa values of 10–20 mm, making the results less reproducible. Figure 12 shows SEM images of the fracture surfaces of 1S–2NF–1 and 2S–1NF–5 samples, respectively, which showed micro-dimples, the presence of nylon cloth, and areas rich in nanofibers. The nanofibers in the sample 2S–1NF appear less stretched and were broken inside the matrix without evident pull-out, resulting in fracture toughness values lower than those of 1S–2NF samples and comparable to those of virgin ones.

Figure 13 shows a comparison of the R-Curves of one representative specimen for each configuration. The black markers identify the G_{IC} values used for calculating the average fracture toughness during the steady-state crack propagation phase, while the grey markers represent the excluded ones. Considering all the specimens tested (see Table 1), the average fracture toughness of the neat adhesive is 0.42 ± 0.07 N/mm for 1S and 0.42 ± 0.10 N/mm for 2S. The average fracture toughness of the nanomodified 1S–2NF series is instead 0.55 ± 0.16 N/mm, while for 2S–1NF, it is about 0.44 ± 0.8 N/mm. The average G_{IC} values are reported in Figure 14. The samples 1S–2NF have more scattered values, but higher average GIC than 2S–1NF. The average maximum load values are reported in Figure 15. Again, the highest maximum load was achieved by the 1S–2NF samples with an average maximum load value of 580 N ± 47 N, which is 10% higher than that of the 1S specimens.

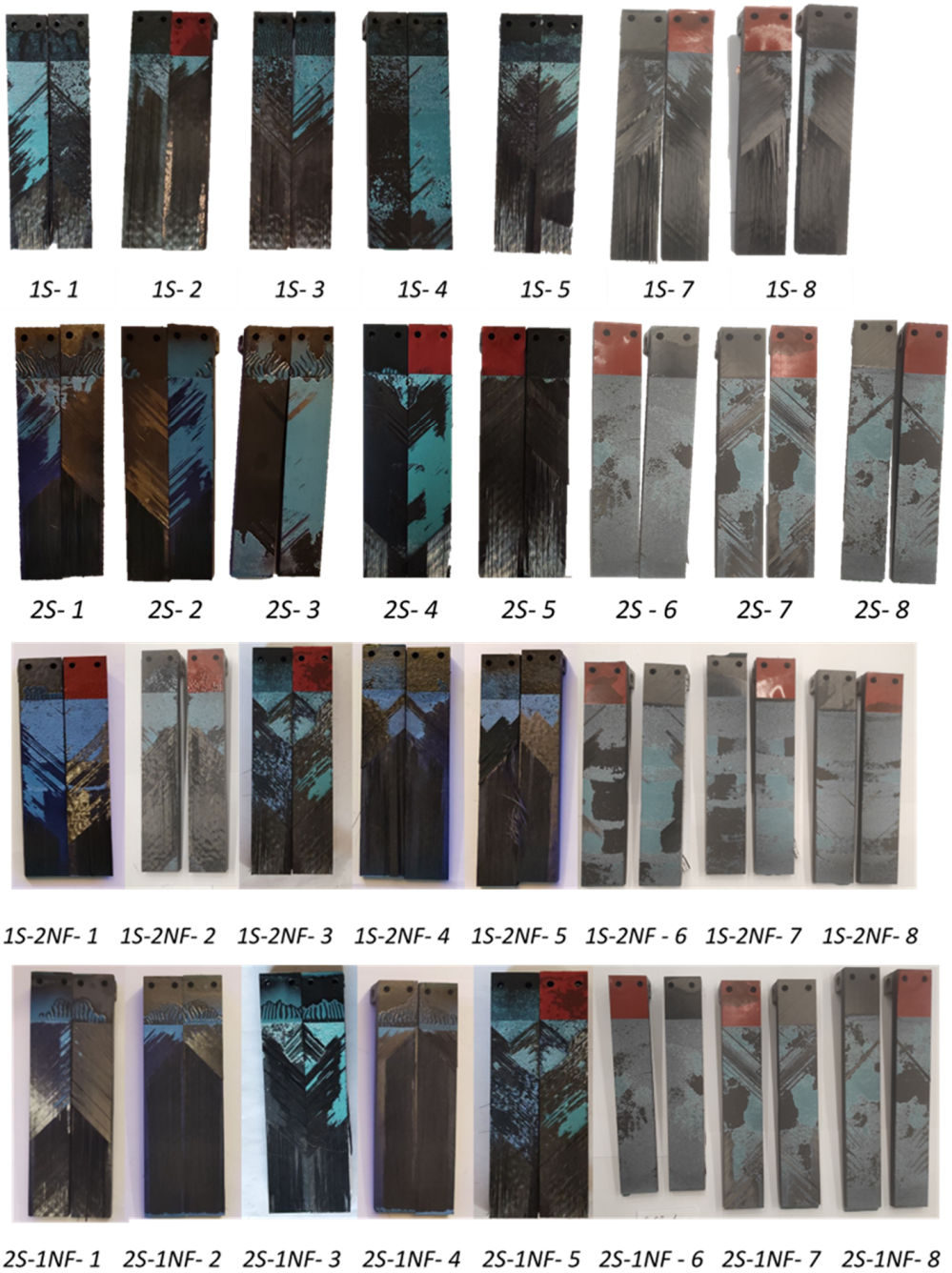

Figure 10. Fracture surface.

The results obtained confirm that the virgin samples exhibit the same fracture toughness values, regardless of the number of adhesive layers used for bonding. The highest values of fracture toughness were obtained by the 1S–2NF samples. Nanofibers placed at the adhesive/adhesive interface deformed and contributed to the joint toughness. The configuration 1S–2NF exhibited a 32% improvement compared to 1S samples. The lower deformation of the nanofibers placed between the two adhesive layers of the 2S–1NF samples resulted in a lower toughness value of the system, which, however, was still comparable with the virgin samples.

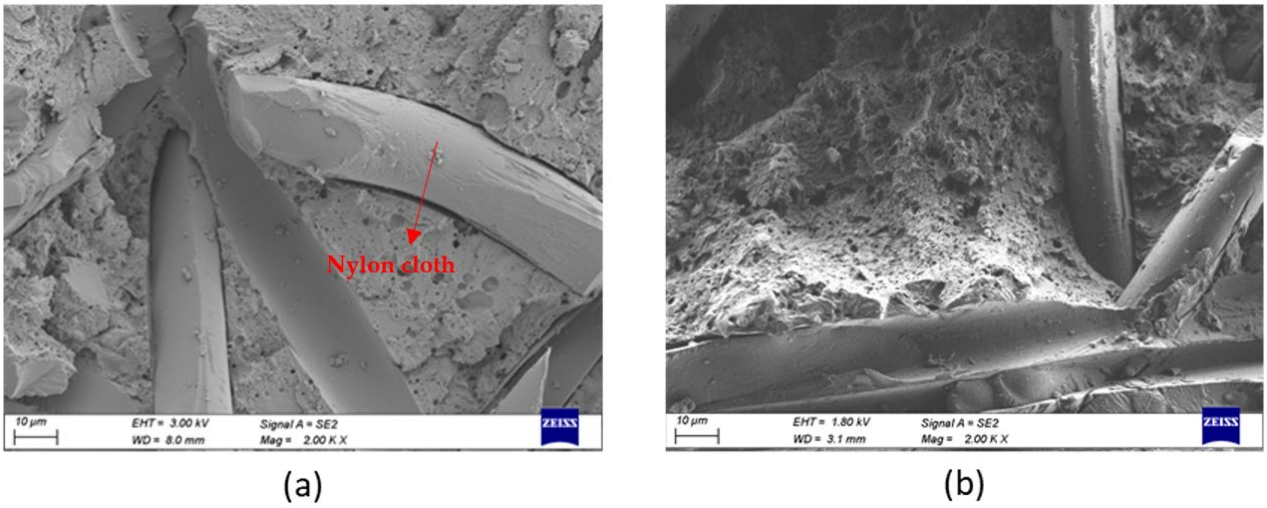

Figure 11. SEM images of fracture surfaces of 1S–1 (**a**) and 2S–6 (**b**) at 2000×.

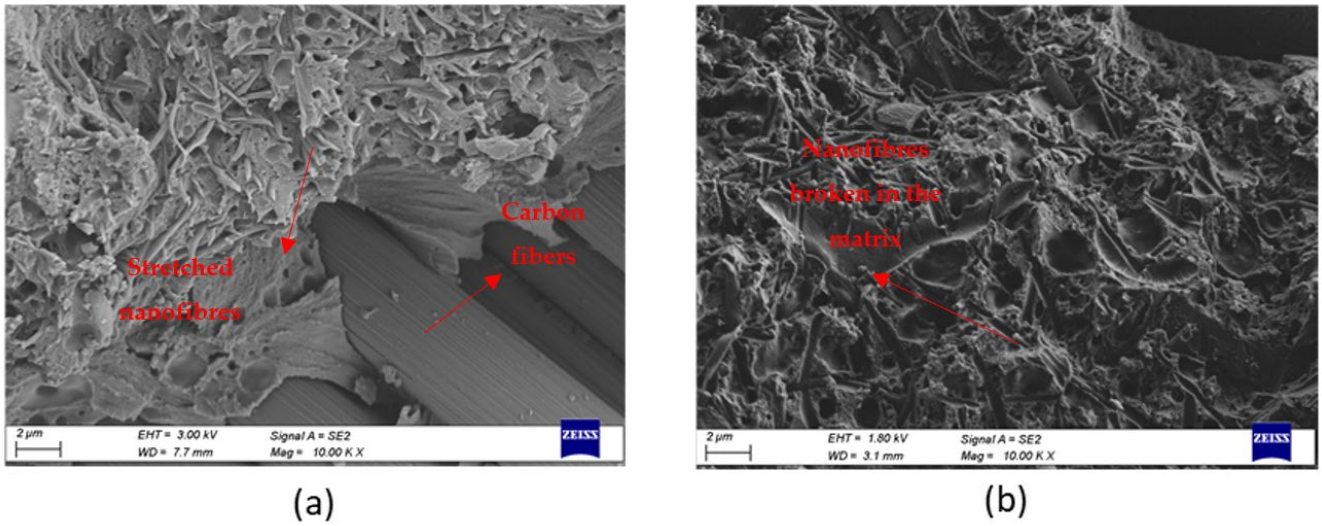

Figure 12. SEM images of fracture surfaces of 1S–NF–1 (**a**) and 2S–1NF–5 (**b**) at 10,000×.

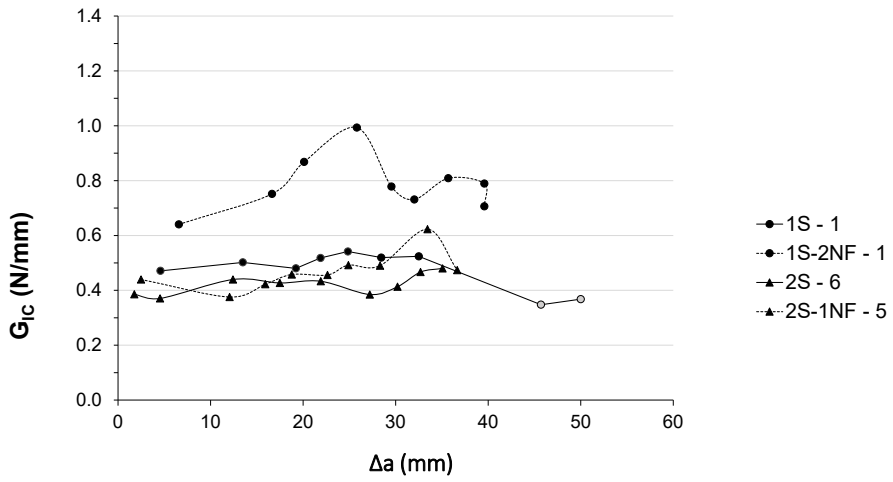

Figure 13. Comparison of R-Curves of representative virgin (1S and 2S) and nanomodified (1S–2NF and 2S–1NF) specimens.

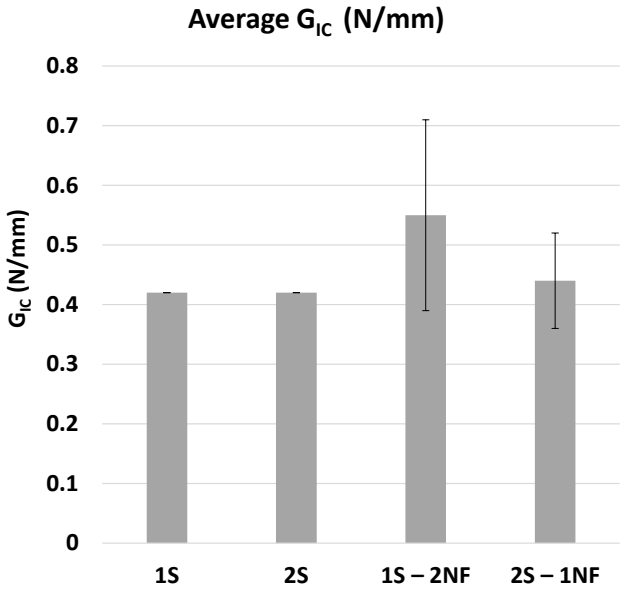

Figure 14. G_{IC} average values for 1S, 2S, 1S–2NF, and 2S–1NF samples.

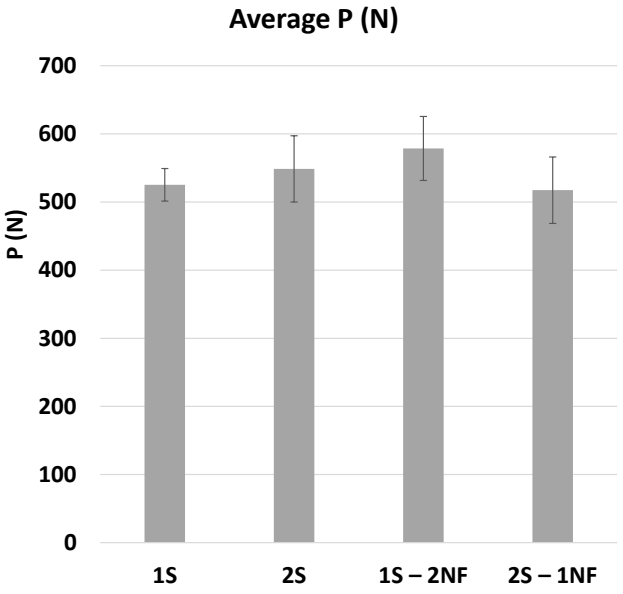

Figure 15. Maximum load average values for 1S, 2S, 1S–2NF, and 2S–1NF samples.

4. Conclusions

The effect of commercial XD10 PA (XantuLayr®) nanofibers within composite joints bonded with the epoxy film was studied. Materials and bonding techniques commonly employed in the automotive and aerospace sector were used for joint manufacturing. Since the adhesive was in film form, nanofiber integration could be approached in two ways. The first was to apply the nanofiber at the adherents/adhesive interface. The second was to interleave the nanomat between two layers of adhesive.

The main results are reported below:

1. The behaviors of virgin samples are similar, and are not influenced by the number of adhesive layers used for bonding;
2. The application of commercial XD10 PA nanofibers (XantuLayr®) at the adhesive/adherent interface improves the mechanical performance of the composite joints, which exhibited higher fracture toughness and fracture resistance than virgin samples. In

particular, the 1S-2NF specimens exhibited 10% and 32% higher maximum strength and fracture toughness values, respectively;

3. SEM images confirm the contribution of the nanofibers that appear elongated and detached from the matrix. The deformation of the nanomat contributes to the joint toughness;
4. The same nanomaterial applied to the center of the adhesive layer does not contribute to the fracture toughness of the joint, as the nanomodified joints show the same G_{IC} and standard deviation values as the virgin samples.

The application of commercial XD10 PA nanofibers (XantuLayr®) was very simple, and is definitely compatible with materials and bonding techniques used for composite materials.

Further developments of this work will involve evaluating mode II fracture toughness through End-Notched-Flexure (ENF). Further analyses could be conducted on thinner substrate bonds by performing T-Peel tests.

Author Contributions: Conceptualization, S.M. and A.P.; methodology, S.M., F.M. and A.P.; software, N/A; validation, A.P. and F.M.; formal analysis, S.M.; investigation, S.M.; resources, S.M., F.M. and A.P.; data curation, S.M.; writing—original draft preparation, S.M.; writing—review and editing, A.P. and S.M.; visualization, S.M.; supervision, A.P.; project administration, N/A; funding acquisition, N/A. All authors have read and agreed to the published version of the manuscript.

Funding: This research received no external funding.

Data Availability Statement: Data is contained within the article.

Conflicts of Interest: The authors declare no conflict of interest.

References

1. Da Silva, L.F.M.; Öchsner, A.; Adams, R.D. (Eds.) *Handbook of Adhesion Technology*; Springer: Berlin/Heidelberg, Germany, 2011; ISBN 978-3-642-01168-9.
2. Kupski, J.; Teixeira de Freitas, S. Design of Adhesively Bonded Lap Joints with Laminated CFRP Adherends: Review, Challenges and New Opportunities for Aerospace Structures. *Compos. Struct.* **2021**, *268*, 113923. [CrossRef]
3. De Oliveira, L.Á.; Vieira, M.M.; dos Santos, J.C.; Freire, R.T.S.; Tonatto, M.L.P.; Panzera, T.H.; Zamani, P.; Scarpa, F. An Investigation on the Mechanical Behaviour of Sandwich Composite Structures with Circular Honeycomb Bamboo Core. *Discov. Mech. Eng.* **2022**, *1*, 7. [CrossRef]
4. Soltannia, B.; Mertiny, P.; Taheri, F. Static and Dynamic Characteristics of Nano-Reinforced 3D-Fiber Metal Laminates Using Non-Destructive Techniques. *J. Sandw. Struct. Mater.* **2021**, *23*, 3081–3112. [CrossRef]
5. Zamani, P.; Jaamialahmadi, A.; da Silva, L.F.M. Fatigue Life Evaluation of Al-GFRP Bonded Lap Joints under Four-Point Bending Using Strain-Life Criteria. *Int. J. Adhes. Adhes.* **2023**, *122*, 103338. [CrossRef]
6. Turan, K.; Örçen, G. Failure Analysis of Adhesive-Patch-Repaired Edge-Notched Composite Plates. *J. Adhes.* **2017**, *93*, 328–341. [CrossRef]
7. Olajide, S.O.; Kandare, E.; Khatibi, A.A. Fatigue Life Uncertainty of Adhesively Bonded Composite Scarf Joints—An Airworthiness Perspective. *J. Adhes.* **2017**, *93*, 515–530. [CrossRef]
8. Rasane, A.R.; Kumar, P.; Khond, M.P. Optimizing the Size of a CFRP Patch to Repair a Crack in a Thin Sheet. *J. Adhes.* **2017**, *93*, 1064–1080. [CrossRef]
9. De Cicco, D.; Taheri, F. Effect of Functionalized Graphene Nanoplatelets on the Delamination-Buckling and Delamination Propagation Resistance of 3D Fiber-Metal Laminates Under Different Loading Rates. *Nanomaterials* **2019**, *9*, 1482. [CrossRef]
10. Gong, Y.; Chen, X.; Zou, L.; Li, X.; Zhao, L.; Zhang, J.; Hu, N. Experimental and Numerical Investigations on the Mode I Delamination Growth Behavior of Laminated Composites with Different Z-Pin Fiber Reinforcements. *Compos. Struct.* **2022**, *287*, 115370. [CrossRef]
11. Neto, J.A.B.P.; Campilho, R.D.S.G.; da Silva, L.F.M. Parametric Study of Adhesive Joints with Composites. *Int. J. Adhes. Adhes.* **2012**, *37*, 96–101. [CrossRef]
12. Dadian, A.; Rahnama, S.; Zolfaghari, A. Experimental Study of the CTBN Effect on Mechanical Properties and Mode I and II Fracture Toughness of a New Epoxy Resin. *J. Adhes. Sci. Technol.* **2020**, *34*, 2389–2404. [CrossRef]
13. Giv, A.N.; Ayatollahi, M.R.; Ghaffari, S.H.; da Silva, L.F.M. Effect of Reinforcements at Different Scales on Mechanical Properties of Epoxy Adhesives and Adhesive Joints: A Review. *J. Adhes.* **2018**, *94*, 1082–1121. [CrossRef]
14. Saraç, İ.; Adin, H.; Temiz, Ş. Experimental Determination of the Static and Fatigue Strength of the Adhesive Joints Bonded by Epoxy Adhesive Including Different Particles. *Compos. Part B Eng.* **2018**, *155*, 92–103. [CrossRef]
15. Banea, M.D.; da Silva, L.F.M.; Carbas, R.J.C.; Campilho, R.D.S.G. Mechanical and Thermal Characterization of a Structural Polyurethane Adhesive Modified with Thermally Expandable Particles. *Int. J. Adhes. Adhes.* **2014**, *54*, 191–199. [CrossRef]

16. Caldona, E.B.; De Leon, A.C.C.; Pajarito, B.B.; Advincula, R.C. A Review on Rubber-Enhanced Polymeric Materials. *Polym. Rev.* **2017**, *57*, 311–338. [CrossRef]
17. Riew, C.K.; Siebert, A.R.; Smith, R.W.; Fernando, M.; Kinloch, A.J. Toughened Epoxy Resins: Preformed Particles as Toughening for Adhesives and Matrices. In *Toughened Plastics II*; Advances in Chemistry; Riew, C.K., Kinloch, A.J., Eds.; American Chemical Society: Washington, DC, USA, 1996; Volume 252, pp. 33–44. ISBN 978-0-8412-3151-1.
18. Williams, R.J.J.; Rozenberg, B.A.; Pascault, J.-P. Reaction-Induced Phase Separation in Modified Thermosetting Polymers. In *Polymer Analysis Polymer Physics*; Advances in Polymer Science; Springer: Berlin/Heidelberg, Germany, 1997; pp. 95–156. ISBN 978-3-540-68374-2.
19. Tsang, W.L.; Taylor, A.C. Fracture and Toughening Mechanisms of Silica- and Core–Shell Rubber-Toughened Epoxy at Ambient and Low Temperature. *J. Mater. Sci* **2019**, *54*, 13938–13958. [CrossRef]
20. Wise, C.W.; Cook, W.D.; Goodwin, A.A. CTBN Rubber Phase Precipitation in Model Epoxy Resins. *Polymer* **2000**, *41*, 4625–4633. [CrossRef]
21. Bagheri, R.; Marouf, B.T.; Pearson, R.A. Rubber-Toughened Epoxies: A Critical Review. *Polym. Rev.* **2009**, *49*, 201–225. [CrossRef]
22. Kinloch, A.J. Toughening Epoxy Adhesives to Meet Today's Challenges. *MRS Bull.* **2003**, *28*, 445–448. [CrossRef]
23. Ghabezi, P.; Farahani, M. Effects of Nanoparticles on Nanocomposites Mode I and II Fracture: A Critical Review. In *Progress in Adhesion and Adhesives*; John Wiley & Sons, Ltd: Hoboken, NJ, USA, 2018; pp. 391–411. ISBN 978-1-119-52644-5.
24. Ghabezi, P.; Farahani, M. A Cohesive Model with a Multi-Stage Softening Behavior to Predict Fracture in Nano Composite Joints. *Eng. Fract. Mech.* **2019**, *219*, 106611. [CrossRef]
25. Yang, G.; OuYang, Q.; Ye, J.; Liu, L. Improved Tensile and Single-Lap-Shear Mechanical-Electrical Response of Epoxy Composites Reinforced with Gridded Nano-Carbons. *Compos. Part A Appl. Sci. Manuf.* **2022**, *152*, 106712. [CrossRef]
26. NajiMehr, H.; Shariati, M.; Zamani, P.; da Silva, L.F.M.; Ghahremani Moghadam, D. Investigating on the Influence of Multi-Walled Carbon Nanotube and Graphene Nanoplatelet Additives on Residual Strength of Bonded Joints Subjected to Partial Fatigue Loading. *J. Appl. Polym. Sci.* **2022**, *139*, 52069. [CrossRef]
27. Demir, K.; Gavgali, E.; Yetim, A.F.; Akpinar, S. The Effects of Nanostructure Additive on Fracture Strength in Adhesively Bonded Joints Subjected to Fully Reversed Four-Point Bending Fatigue Load. *Int. J. Adhes. Adhes.* **2021**, *110*, 102943. [CrossRef]
28. Zamani, P.; Jaamialahmadi, A.; da Silva, L.F.M. The Influence of GNP and Nano-Silica Additives on Fatigue Life and Crack Initiation Phase of Al-GFRP Bonded Lap Joints Subjected to Four-Point Bending. *Compos. Part B Eng.* **2021**, *207*, 108589. [CrossRef]
29. Takeda, T.; Narita, F. Fracture Behavior and Crack Sensing Capability of Bonded Carbon Fiber Composite Joints with Carbon Nanotube-Based Polymer Adhesive Layer under Mode I Loading. *Compos. Sci. Technol.* **2017**, *146*, 26–33. [CrossRef]
30. Khoramishad, H.; Khakzad, M. Toughening Epoxy Adhesives with Multi-Walled Carbon Nanotubes. *J. Adhes.* **2018**, *94*, 15–29. [CrossRef]
31. Akpinar, I.A.; Gürses, A.; Akpinar, S.; Gültekin, K.; Akbulut, H.; Ozel, A. Investigation of Mechanical and Thermal Properties of Nanostructure-Doped Bulk Nanocomposite Adhesives. *J. Adhes.* **2018**, *94*, 847–866. [CrossRef]
32. Jojibabu, P.; Zhang, Y.X.; Rider, A.N.; Wang, J.; Gangadhara Prusty, B. Synergetic Effects of Carbon Nanotubes and Triblock Copolymer on the Lap Shear Strength of Epoxy Adhesive Joints. *Compos. Part B Eng.* **2019**, *178*, 107457. [CrossRef]
33. Cha, J.; Kim, J.; Ryu, S.; Hong, S.H. Comparison to Mechanical Properties of Epoxy Nanocomposites Reinforced by Functionalized Carbon Nanotubes and Graphene Nanoplatelets. *Compos. Part B Eng.* **2019**, *162*, 283–288. [CrossRef]
34. Xu, L.R.; Li, L.; Lukehart, C.; Kuai, H. Mechanical Characterization of Nanofiber-Reinforced Composite Adhesives. *J. Nanosci. Nanotechnol.* **2007**, *7*, 2546–2548. [CrossRef]
35. Sam-Daliri, O.; Farahani, M.; Araei, A. Condition Monitoring of Crack Extension in the Reinforced Adhesive Joint by Carbon Nanotubes. *Weld. Technol. Rev.* **2020**, *91*, 7–15. [CrossRef]
36. Burch, K.; Doshi, S.; Chaudhari, A.; Thostenson, E.; Higginson, J. Estimating Ground Reaction Force with Novel Carbon Nanotube-Based Textile Insole Pressure Sensors. *Wearable Technol.* **2023**, *4*, e8. [CrossRef] [PubMed]
37. Sam-Daliri, O.; Farahani, M.; Faller, L.-M.; Zangl, H. Structural Health Monitoring of Defective Single Lap Adhesive Joints Using Graphene Nanoplatelets. *J. Manuf. Process.* **2020**, *55*, 119–130. [CrossRef]
38. Çakır, M.V.; Özbek, Ö. Mechanical Performance and Damage Analysis of GNP-Reinforced Adhesively Bonded Joints under Shear and Bending Loads. *J. Adhes.* **2023**, *99*, 869–892. [CrossRef]
39. Stetco, C.; Sam-Daliri, O.; Faller, L.-M.; Zangl, H. Piezocapacitive Sensing for Structural Health Monitoring in Adhesive Joints. In Proceedings of the 2019 IEEE International Instrumentation and Measurement Technology Conference (I2MTC), Auckland, New Zealand, 20–23 May 2019; pp. 1–5.
40. Radshad, H.; Khoramishad, H.; Nazari, R. The Synergistic Effect of Hybridizing and Aligning Graphene Oxide Nanoplatelets and Multi-Walled Carbon Nanotubes on Mode-I Fracture Behavior of Nanocomposite Adhesive Joints. *Proc. Inst. Mech. Eng. Part L J. Mater. Des. Appl.* **2022**, *236*, 1764–1776. [CrossRef]
41. Çakır, M.V. The Synergistic Effect of Hybrid Nano-Silica and GNP Additives on the Flexural Strength and Toughening Mechanisms of Adhesively Bonded Joints. *Int. J. Adhes. Adhes.* **2023**, *122*, 103333. [CrossRef]
42. Zamani, P.; FM da Silva, L.; Masoudi Nejad, R.; Ghahremani Moghaddam, D.; Soltannia, B. Experimental Study on Mixing Ratio Effect of Hybrid Graphene Nanoplatelet/Nano-Silica Reinforcement on the Static and Fatigue Life of Aluminum-to-GFRP Bonded Joints under Four-Point Bending. *Compos. Struct.* **2022**, *300*, 116108. [CrossRef]

43. Zamani, P.; Alaei, M.H.; da Silva, L.F.M.; Ghahremani-Moghadam, D. On the Static and Fatigue Life of Nano-Reinforced Al-GFRP Bonded Joints under Different Dispersion Treatments. *Fatigue Fract. Eng. Mater. Struct.* **2022**, *45*, 1088–1110. [CrossRef]
44. Özbek, Ö.; Çakır, M.V. MWCNT and Nano-Silica Hybrids Effect on Mechanical and Fracture Characterization of Single Lap Joints of GFRP Plates. *Int. J. Adhes. Adhes.* **2022**, *117*, 103159. [CrossRef]
45. Huang, Z.-M.; Zhang, Y.-Z.; Kotaki, M.; Ramakrishna, S. A Review on Polymer Nanofibers by Electrospinning and Their Applications in Nanocomposites. *Compos. Sci. Technol.* **2003**, *63*, 2223–2253. [CrossRef]
46. Palazzetti, R.; Zucchelli, A. Electrospun Nanofibers as Reinforcement for Composite Laminates Materials—A Review. *Compos. Struct.* **2017**, *182*, 711–727. [CrossRef]
47. Hamer, S.; Leibovich, H.; Intrater, R.; Zussman, E.; Siegmann, A.; Sherman, D. Mode I Interlaminar Fracture Toughness of Nylon 66 Nanofibrilmat Interleaved Carbon/Epoxy Laminates. *Polym. Compos.* **2011**, *32*, 1781–1789. [CrossRef]
48. Moroni, F.; Palazzetti, R.; Zucchelli, A.; Pirondi, A. A Numerical Investigation on the Interlaminar Strength of Nanomodified Composite Interfaces. *Compos. Part B Eng.* **2013**, *55*, 635–641. [CrossRef]
49. Beckermann, G.W.; Pickering, K.L. Mode I and Mode II Interlaminar Fracture Toughness of Composite Laminates Interleaved with Electrospun Nanofibre Veils. *Compos. Part A Appl. Sci. Manuf.* **2015**, *72*, 11–21. [CrossRef]
50. Saghafi, H.; Palazzetti, R.; Zucchelli, A.; Minak, G. Influence of Electrospun Nanofibers on the Interlaminar Properties of Unidirectional Epoxy Resin/Glass Fiber Composite Laminates. *J. Reinf. Plast. Compos.* **2015**, *34*, 907–914. [CrossRef]
51. Daelemans, L.; van der Heijden, S.; De Baere, I.; Rahier, H.; Van Paepegem, W.; De Clerck, K. Using Aligned Nanofibres for Identifying the Toughening Micromechanisms in Nanofibre Interleaved Laminates. *Compos. Sci. Technol.* **2016**, *124*, 17–26. [CrossRef]
52. Daelemans, L.; van der Heijden, S.; De Baere, I.; Rahier, H.; Van Paepegem, W.; De Clerck, K. Improved Fatigue Delamination Behaviour of Composite Laminates with Electrospun Thermoplastic Nanofibrous Interleaves Using the Central Cut-Ply Method. *Compos. Part A Appl. Sci. Manuf.* **2017**, *94*, 10–20. [CrossRef]
53. Beckermann, G.W. Nanofiber Interleaving Veils for Improving the Performance of Composite Laminates. *Reinf. Plast.* **2017**, *61*, 289–293. [CrossRef]
54. Goodarz, M.; Bahrami, S.H.; Sadighi, M.; Saber-Samandari, S. Low-Velocity Impact Performance of Nanofiber-Interlayered Aramid/Epoxy Nanocomposites. *Compos. Part B Eng.* **2019**, *173*, 106975. [CrossRef]
55. Oh, H.J.; Kim, H.Y.; Kim, S.S. Effect of the Core/Shell-Structured Meta-Aramid/Epoxy Nanofiber on the Mechanical and Thermal Properties in Epoxy Adhesive Composites by Electrospinning. *J. Adhes.* **2014**, *90*, 787–801. [CrossRef]
56. On, S.Y.; Kim, M.S.; Kim, S.S. Effects of Post-Treatment of Meta-Aramid Nanofiber Mats on the Adhesion Strength of Epoxy Adhesive Joints. *Compos. Struct.* **2017**, *159*, 636–645. [CrossRef]
57. Razavi, S.M.J.; Neisiany, R.E.; Ayatollahi, M.R.; Ramakrishna, S.; Khorasani, S.N.; Berto, F. Fracture Assessment of Polyacrylonitrile Nanofiber-Reinforced Epoxy Adhesive. *Theor. Appl. Fract. Mech.* **2018**, *97*, 448–453. [CrossRef]
58. Ekrem, M.; Avcı, A. Effects of Polyvinyl Alcohol Nanofiber Mats on the Adhesion Strength and Fracture Toughness of Epoxy Adhesive Joints. *Compos. Part B Eng.* **2018**, *138*, 256–264. [CrossRef]
59. Musiari, F.; Pirondi, A.; Moroni, F.; Giuliese, G.; Belcari, J.; Zucchelli, A.; Brugo, T.M.; Minak, G.; Ragazzini, C. Feasibility Study of Adhesive Bonding Reinforcement by Electrospun Nanofibers. *Procedia Struct. Integr.* **2016**, *2*, 112–119. [CrossRef]
60. Musiari, F.; Pirondi, A.; Zucchelli, A.; Menozzi, D.; Belcari, J.; Brugo, T.M.; Zomparelli, L. Experimental Investigation on the Enhancement of Mode I Fracture Toughness of Adhesive Bonded Joints by Electrospun Nanofibers. *J. Adhes.* **2018**, *94*, 974–990. [CrossRef]
61. Brugo, T.; Musiari, F.; Pirondi, A.; Zucchelli, A.; Cocchi, D.; Menozzi, D. Development and Fracture Toughness Characterization of a Nylon Nanomat Epoxy Adhesive Reinforcement. *Proc. Inst. Mech. Eng.* **2018**, *233*, 465–474. [CrossRef]
62. Cocchi, D.; Musiari, F.; Brugo, T.M.; Pirondi, A.; Zucchelli, A.; Campanini, F.; Leoni, E.; Mazzocchetti, L. Characterization of Aluminum Alloy-Epoxy Bonded Joints with Nanofibers Obtained by Electrospinning. *J. Adhes.* **2020**, *96*, 384–401. [CrossRef]
63. *ASTM D3039/D3039M-08*; Standard Test Method for Tensile Properties of Polymer Matrix Composite Materials. ASTM International: West Conshohocken, PA, USA, 2014.
64. Han, X.; Jin, Y.; da Silva, L.F.M.; Costa, M.; Wu, C. On the Effect of Adhesive Thickness on Mode I Fracture Energy—An Experimental and Modelling Study Using a Trapezoidal Cohesive Zone Model. *J. Adhes.* **2020**, *96*, 490–514. [CrossRef]
65. Yan, C.C.; Ma, J.L.; Zhang, Y.X.; Wu, C.W.; Yang, P.; Wang, P.; Zhang, W.; Han, X. The Fracture Performance of Adhesively Bonded Orthodontic Brackets: An Experimental-FE Modelling Study. *J. Adhes.* **2020**, *98*, 180–206. [CrossRef]
66. Fernández, M.V.; de Moura, M.F.S.F.; da Silva, L.F.M.; Marques, A.T. Composite Bonded Joints under Mode I Fatigue Loading. *Int. J. Adhes. Adhes.* **2011**, *31*, 280–285. [CrossRef]
67. Gunnion, A.J.; Herszberg, I. Parametric Study of Scarf Joints in Composite Structures. *Compos. Struct.* **2006**, *75*, 364–376. [CrossRef]
68. Xu, Y.; He, Q.; Yang, W.; Sun, T.; Tang, Q. Study on Relationships between Curing Pressures and Mechanical Properties for Epoxy Adhesive Films. *Chem. Eng. Trans.* **2018**, *66*, 43–48. [CrossRef]
69. Xie, Z.; Wang, S.; Li, X. *Composite Tapered Scarf Joint Repair: Analytical Model and Experimental Validation*; Atlantis Press: Amsterdam, The Netherlands, 2016; pp. 720–726.
70. Krenk, S. Energy Release Rate of Symmetric Adhesive Joints. *Eng. Fract. Mech.* **1992**, *43*, 549–559. [CrossRef]

71. Minosi, S.; Cocchi, D.; Pirondi, A.; Zucchelli, A.; Campanini, F. Integration of Nylon Electrospun Nanofibers into Structural Epoxy Adhesive Joints. *IOP Conf. Ser. Mater. Sci. Eng.* **2021**, *1038*, 012048. [CrossRef]
72. Minosi, S.; Cocchi, D.; Maccaferri, E.; Pirondi, A.; Zucchelli, A.; Mazzocchetti, L.; Ambrosini, D.; Campanini, F. Exploitation of Rubbery Electrospun Nanofibrous Mat for Fracture Toughness Improvement of Structural Epoxy Adhesive Bonded Joints. *J. Adv. Join. Process.* **2021**, *3*, 100050. [CrossRef]